

Yan Cheng · Guan Wang · Manming Yan · Zhiyu Jiang

In situ analysis of interfacial reactions between negative MCMB, lithium electrodes, and gel polymer electrolyte

Received: 18 November 2005 / Revised: 26 January 2006 / Accepted: 10 February 2006 / Published online: 28 March 2006
© Springer-Verlag 2006

Abstract The interfacial properties of mesocarbon-microbeads (MCMB) and lithium electrodes during charge process in poly (vinylidenefluoride-co-hexafluoropropylene)-based gel electrolyte were investigated by in situ Raman microscopy, in situ Fourier transform-infrared (FTIR) spectroscopic methods, and charge-discharge, electrochemical impedance spectroscopy techniques. For MCMB electrode, the series phase transitions from initial formation of the dilute stage 1 graphite intercalation compound (GIC) to a stage 4 GIC, then through a stage 3 to stage 2, and finally to stage 1 GIC was proved by in situ Raman spectroscopic measurement. The formation of solid electrolyte interface (SEI) films formed on MCMB and metal lithium electrode was studied by in situ reflectance FTIR spectroscopic method. At MCMB electrode surface, the solvent (mostly ethylene carbonate) decomposed during charging process and ROCO_2Li may be the product. ROCO_2Li , ROLi , and Li_2CO_3 were the main composites of SEI film formed on lithium electrode, not on electro-deposited lithium electrode or lithium foil electrode.

Keywords In situ Raman spectroscopy · In situ FTIR spectroscopy · Solid electrolyte interface · Gel electrolyte · Mesocarbon microbeads

Introduction

Gel polymer electrolytes (GPE) are considered as promising candidates for high-energy electrochemical devices and have long been investigated for their use in polymer

electrolyte lithium battery and lithium ion battery. A great deal of effort was invested in the synthesis of gel electrolytes for lithium and lithium ion batteries and their application in practical rechargeable batteries [1–7]. However, the interfacial studies of carbon and lithium electrodes in contact with gel electrolyte systems are still rarely reported.

As carbonaceous materials are concerned, both structural variations of carbon materials during lithium intercalation-deintercalation processes and the characteristics of solid electrolyte interface (SEI) film formed on the electrode surface by the reduction-decomposition of the electrolyte are some of the most critical factors to affect the performances of lithium ion batteries. In view of lithium metal electrode, the thermodynamic instability in contact with most organic electrolytes leads to a formation of SEI layers on the electrode surface. SEI film can be formed on the lithium metal surface through the reaction of lithium with trace water, organic solvent, and some impurities. It acts a quite important role between lithium electrode and polymer electrolyte, which may determine battery behavior such as cycle performance and safety. The mechanisms of SEI formation and lithium transport through SEI are rather complex and are still a subject of controversial scientific discussions although they were extensively investigated by Fourier transform-infrared (FTIR), high resolution transmission electron microscopy, scanning electronic micrograph, X-ray photoelectron spectroscopy, atomic force microscopy, and electrochemical methods [8–22].

In the present work, in situ spectroscopic methods (Raman and FTIR spectroscopy) and electrochemical techniques were employed to investigate the interfacial characteristics of mesocarbon-microbeads (MCMB) electrode surface and lithium metal electrode surface in poly (vinylidenefluoride-co-hexafluoropropylene) [$\text{P}(\text{VdF-HFP})$]-based gel electrolyte. Electrochemical performances of MCMB electrode in the gel electrolyte were obtained through charge-discharge test and electrochemical impedance spectra (EIS) measurements. Structural changes of MCMB material in the initial lithium intercalation process were studied by in situ

Y. Cheng · G. Wang · M. Yan · Z. Jiang (✉)
Department of Chemistry, Fudan University,
Shanghai 200433, People's Republic of China
e-mail: zyjiang@fudan.ac.cn
Tel.: +86-21-65642404
Fax: +86-21-65641740

Y. Cheng · G. Wang · M. Yan · Z. Jiang
Shanghai Key Laboratory of Molecular Catalysis
and Innovative Materials, Fudan University,
Shanghai 200433, People's Republic of China

Raman microscopy. SEI formation on the MCMB and lithium metal electrode was analyzed by in situ reflectance FTIR spectroscopic technique.

Experimental

Gel electrolyte preparation

The gel electrolyte was prepared using P (VdF-HFP) produced by Elf Atochem. and the organic electrolyte plasticizer consisting of 1 mol/l LiPF₆ in 50/50 (w/w) ethylene carbonate:diethyl carbonate (EC-DEC). The gel electrolyte was prepared by mixing P (VdF-HFP) with organic electrolyte in the ratio of 30/70 (w/w). The mixture was added to a flask in the dry glove box and then stirred at room temperature until the gel became homogeneous.

Electrochemical measurements

Composite MCMB electrode was prepared as working electrode from a mixture of 90wt% MCMB, 5wt% poly (tetrafluoroethylene) binder, and 5wt% carbon black. Thin copper foils were used as substrate. Lithium foils were used both as counter and reference electrode. EIS and charge-discharge profiles were carried out in a three-electrode cell by using a CHI660 electrochemical working station.

Ion conductivity of the gel electrolyte was evaluated by EIS measurement at room temperature over the frequency range of 100 mHz–100 kHz at a perturbation signal of 5 mV. In the glove box, the gel electrolyte was sandwiched between two stainless steel electrodes with the area of 1.81 cm². The distance between two stainless steel electrodes was fixed at 0.268 cm. The electrochemical behavior of MCMB electrode was also investigated by EIS measurement using the same frequency and perturbation voltage as described previously. EIS measurements were carried out using Potentiostat/Galvanostat EG&G Model 273A frequency response analyzer. Fitting of the impedance spectra to the proposed equivalent circuit was performed by the code Zview program.

Fig. 1 Schematic drawing of in situ Raman spectroscopic cell

In situ Raman microscopy

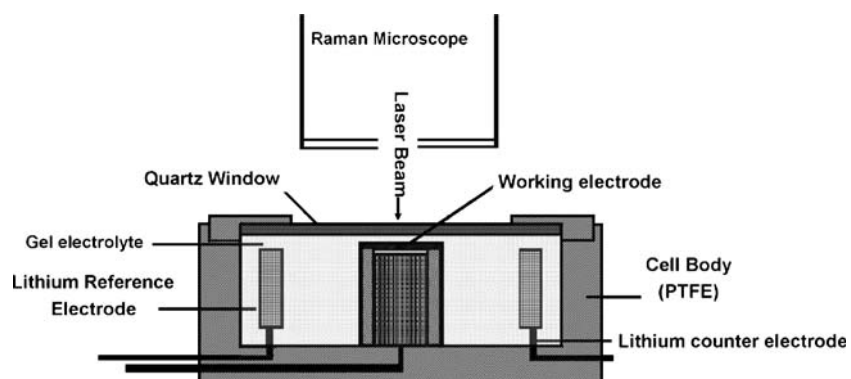
In situ Raman spectra data were collected at room temperature by a confocal Raman microscope (LabRam, Dilor/Instruments). Figure 1 shows a schematic drawing of a homemade in situ Raman spectra cell. At first the cell was dried in a vacuum at 90 °C for 24 h, then filled with gel electrolyte, and sealed strictly in the glove box. In the in situ Raman measurement with the magnification of 50, the laser beam was focused on a small selected surface area. The exciting light source was from a He-Ne Laser with a wavelength of 632.8 nm and intensity below 6 mW.

In situ reflectance FTIR spectroscopy

In situ infrared experiment was performed using a Nicolet 760 FTIR spectrometer equipped with a mercury cadmium telluride-A detector. A thin-layer reflectance cell was used with a similar structure as in situ Raman cell but with the use of a piece of optical NaCl as the window. The cell was dried, assembled, and sealed in dry box. The highest intensity of reflected IR beam was obtained by carefully adjusting the position of electrochemical-spectroscopic cell and the reflecting mirrors. The potential of working electrode was varied step by step. A series of reflection FTIR spectra were measured at each constant potential when current decreased to a stable value. Each spectrum was recorded by accumulating 64 scans with a resolution of 4 cm⁻¹. The reflectance spectra $R(v)$ were calculated as $R(v)=R_{En}(v)/R_{En-1}(v)$ where $R_{En}(v)$ and $R_{En-1}(v)$ refer to the spectra recorded at two neighboring potentials, respectively.

Results and discussion

Ion conductivity of the P (VdF-HFP)-based gel electrolyte
The typical impedance Nyquist plot for the prepared gel electrolyte is shown in Fig. 2. It is a sloping line, which is similar to that the impedance spectra measured for solid polymer electrolyte in our previous paper [23]. The intercept of the sloping line at the high frequency side on the real axis (Z') gives the resistance of gel polymer



layer R_m . Then the conductivity of the electrolyte can be evaluated based on the following relationship:

$$\sigma = \frac{1}{R_m} \cdot \frac{L}{A}$$

where L and A are the thickness and the area of the gel electrolyte, respectively. Herein the conductivity of the prepared gel electrolyte at room temperature is calculated about $4.49 \times 10^{-3} S \cdot cm^{-1}$.

Charge-discharge behavior of MCMB electrode The initial charge-discharge behavior of MCMB in P (VdF-HFP)-based gel electrolyte is shown in Fig. 3a. At the beginning, the potential of MCMB electrode dropped quickly from about 2.9 to 0.8 V because almost no reaction can happen in this potential range. The decrease of potential comes slowly in the potential region of 0.8–0.3 V. It may be corresponding to the formation of SEI layer. In further charging, three visible plateaus were observed at about 170, 100, and 50 mV as displayed in the enlarged plots (Fig. 3b). Zhang and Shi [24] also observed similar three potential plateaus at 190, 110, and 70 mV on the charge curve of MCMB electrode in poly(ethylene glycol) dimethacrylate-based gel electrolyte and proposed that these stages correspond to the phase transitions of GICs from dilute stage 1 to 4, stage 2L to 2, and stage 2 to 1, respectively [25, 26]. During the deintercalation reaction, similar plateaus exist corresponding to the inverse stage transitions. The initial discharge capacity of MCMB is 252.2 mAh g^{-1} and the irreversible capacity in the first charge/discharge cycle is about 50 mAh g^{-1} .

Structural variation of MCMB in the initial lithium intercalation process Raman spectroscopic method proved to be a powerful technique in studying the structures of

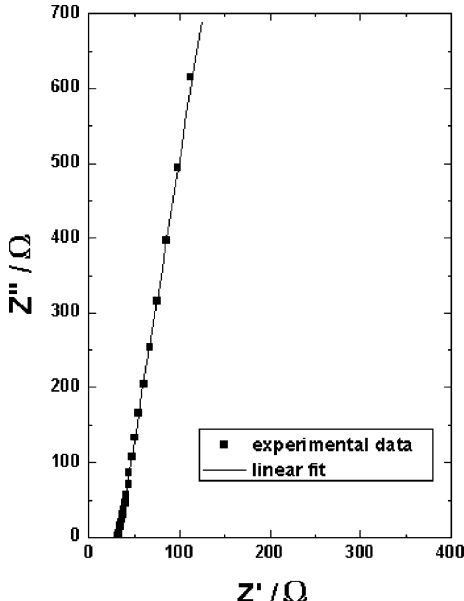


Fig. 2 Nyquist plot for the P (VdF-HFP)-based gel electrolyte at room temperature

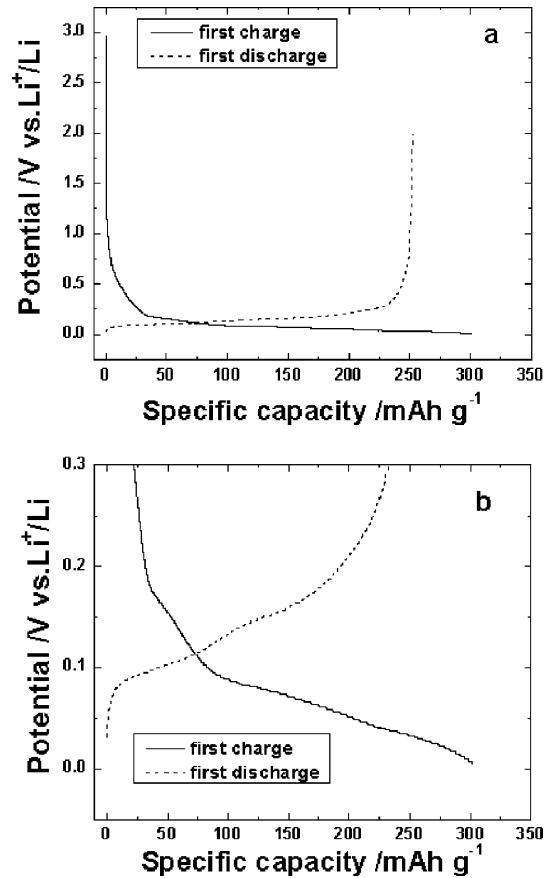


Fig. 3 Charge-discharge profile of the MCMB electrode in the P (VdF-HFP)-based gel electrolyte

graphite materials. The E_{2g} modes corresponding to the in-plane vibrations of the carbon atoms are Raman-active in first-order scattering, which can be observed at approximately 42 cm^{-1} (E_{2g1}) and $1,581 \text{ cm}^{-1}$ (E_{2g2}) [27, 28]. Only the E_{2g2} vibration mode of graphite was investigated in this paper. Figure 4 presents the in situ microscope Raman spectra measured at different potential for MCMB electrode in P (VdF-HFP)-based gel electrolyte during the initial charge process. The relationship between peak shift and the potential is presented in Fig. 5.

The pristine MCMB has an E_{2g2} band centered at $1,576 \text{ cm}^{-1}$ with a full-width-at-half-height bandwidth of 19 cm^{-1} (Fig. 4a). This band starts to narrow at about 0.8 V with the bandwidth of 12 cm^{-1} . Thereafter, in the potential range 0.6–0.3 V, this band gradually shifts to a higher frequency, which indicates the starting of lithium intercalation into MCMB. When the potential decreases to about 0.6 V, the dilute stage 1 phase is formed in which the intercalated Li ions distribute between the graphite layer randomly. The frequency shift of E_{2g2} band is probably ascribed to the increase of the force constant of the in-plane C–C bonds accompanied by the lithium intercalation into graphite [28]. When the potential is stepped to about 0.3 V (Fig. 4b), the band broadens and moves to a higher frequency ($1,591 \text{ cm}^{-1}$). When the potential further decreases to about 0.25 V, two side bands at $1,587 \text{ cm}^{-1}$ [E_{2g2} (i)] and $1,599 \text{ cm}^{-1}$ [E_{2g2} (b)] appear.

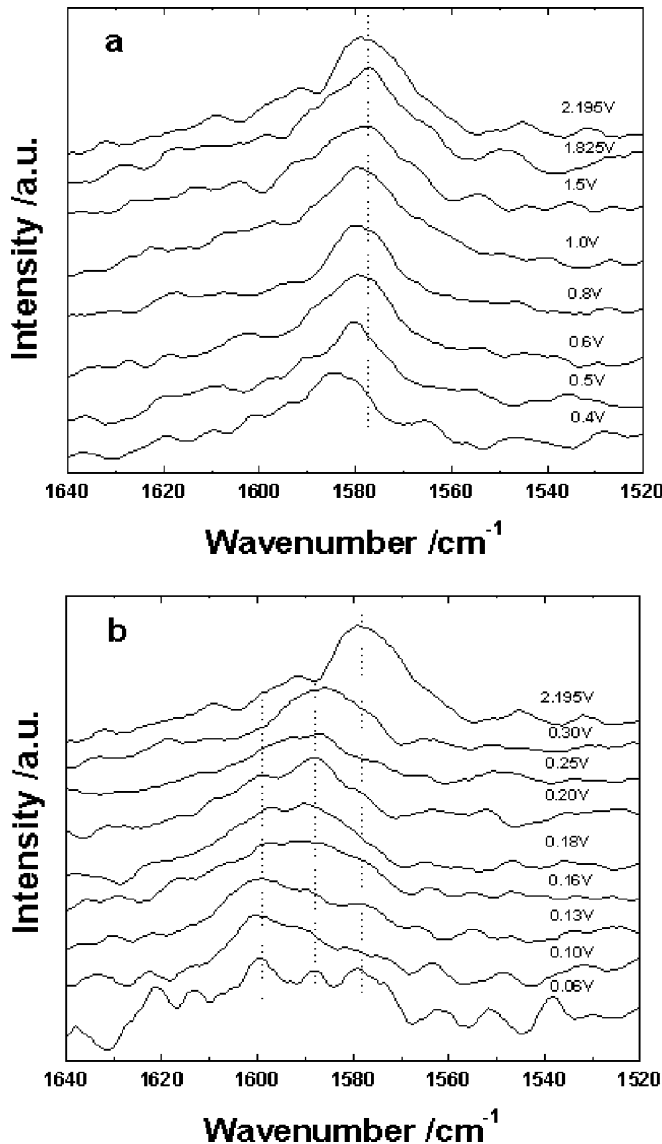


Fig. 4 In situ Raman spectra of MCMB electrode during the initial lithium intercalation process in the P (VdF-HFP)-based gel electrolyte

The E_{2g2} (i) and E_{2g2} (b) modes can be assigned to the vibration of carbon atom in interior graphite layer planes and in bounding graphite layers, respectively. The split of the band indicates the phase transition from the dilute stage 1 phase to the stage 4 phase. After that the peak position of [E_{2g2} (i)] and [E_{2g2} (b)] were approximately kept constant. The intensity of the interior graphite mode [E_{2g2} (i)] decreases in the first instance and then that of the bounding graphite mode [E_{2g2} (b)] decreases with the decrease of the potential in the region 0.2–0.06 V. At 60 mV the intensity of E_{2g2} (i) and E_{2g2} (b) modes become so low that it even misses in the signal noise ultimately. These Raman spectra changes indicate that the phase transition of GICs from stage 4 through stage 3 [intensity decrease of E_{2g2} (i) band], stage 2 [single E_{2g2} (b) band], and to stage 1 [disappearance of E_{2g2} (b) band] in the end [28, 29]. The in situ Raman spectroscopic

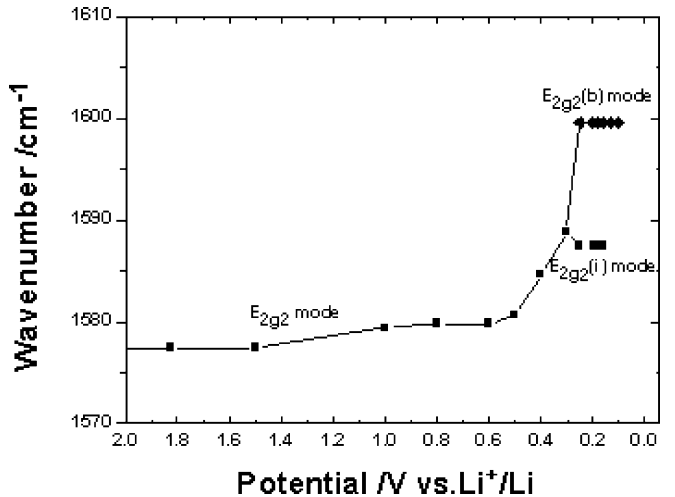


Fig. 5 The relationship between the peak position of E_{2g} mode and the potential

results are coincident with that of the initial charge profile displayed in Fig. 3.

Figure 6 displays the selected in situ Raman spectra recorded at different potentials in the first discharge process. Reversible spectral changes can be observed compared with those presented in Fig. 4. Two bands appear at 0.25 V and become a single band located at 1,584 cm⁻¹ at the potential of 0.6 V. After that the band shifts to lower frequency and reaches 1,578 cm⁻¹ ultimately at 1.89 V. The above spectral information indicates that the phase transitions of MCMB in the prepared P (VdF-HFP)-based gel electrolyte are reversible during the lithium intercalation and deintercalation cycle.

EIS measurements on MCMB electrode during the charge process Figures 7a–c and 8a–c display the selected impedance spectra of MCMB electrode at different potentials during the initial and fourth charge process,

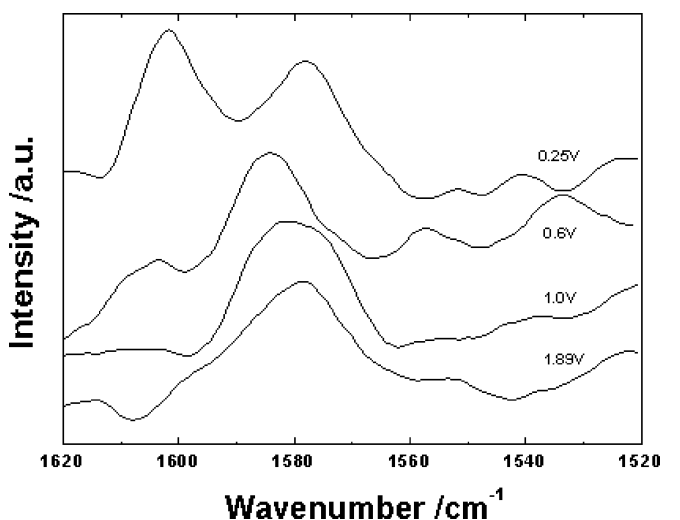


Fig. 6 The selected in situ Raman spectra of MCMB electrode during the initial lithium deintercalation process in the P (VdF-HFP)-based gel electrolyte

respectively, in P (VdF-HFP)-based gel electrolyte. For the initial charge process, the Nyquist plot at the open circuit potential (3.21 V) (Fig. 7a) presents a steep line, which presents the characteristic behavior of double layer capacity. At potential 1.4 V, it presents a half-baked semicircle with a relatively long diameter. When the potential moves to 0.7 V, the semicircle shrinks dramatically. Meanwhile, another very small, depressed semicircle in high frequency region appears on the curve and may indicate the starting of SEI layer formation. The semicircle in the middle frequency region may reflect the properties of lithium–ion intercalation reaction. The diameter of the semicircle in the middle frequency region further reduces in the potential region of 0.7 to 0.2 V (Fig. 7b,c), indicating the increase of activity of lithium intercalation reaction in MCMB electrode. It is interesting to note that the impedance spectra obviously “shift” to the right direction when the potential is below 0.2 V and suggest the increase of R_e about 20 Ω , which may be due to the depletion of ions near the working electrode because of the low diffusion rate in the gel electrolyte. Figure 8a–c shows the similar EIS results for the fourth charge process. It is necessary here to fit the experimental impedance spectra to get a better understanding and comprehension about the lithium intercalation process.

It was generally accepted that the impedance spectra for lithium intercalation to graphite consist of two depressed semicircles with a Warburg-like line [12, 24, 30, 31]. The equivalent circuit used to fit the impedance spectra in this paper is depicted in Fig. 9 where R_e represents the resistance of the electrolyte and R_{SEI} and R_{ct} are the resistance of SEI film and that of charge transfer reaction, respectively. Q_{SEI} and Q_{ct} are the constant phase elements (CPEs) for SEI film and gel electrolyte/MCMB interface, respectively. They mainly correspond to the capacity of SEI film and double layer capacity, respectively. W refers to Warburg resistance. During the simulation of two semicircles, Warburg resistance can be neglected because it is in the low frequency region of EIS.

Figure 10a,b shows the parameter variations of R_{SEI} and R_{ct} . During first charging, R_{SEI} increases from 0.4 to 0.1 V, which indicates the thickening process of SEI film (see Fig. 10a). During the further charging, R_{SEI} drops

obviously when the potential is lower than 0.1 V. It may be because the outside of SEI film becomes porous or due to the stretching of the film by the expanding of the graphite. For the fourth intercalation, R_{SEI} almost remains constant in the broad potential range (0.6–0.3 V), which suggests that SEI film forms stably during the three cycles. When the potential is lower than 0.3 V, R_{SEI} decreases, which is similar to the result in the initial charging process. As shown in Fig. 10b, the variations of R_{ct} in the initial and the fourth charge processes are very similar, which decreases greatly from open circuit potential to about 0.1 V, then it varied slightly.

SEI formation on MCMB electrode investigated by *in situ* reflectance FTIR spectroscopy In situ infrared spectroscopy is an ideal method to analyze the formation of surface film because of its high molecular sensitivity. Figure 11 presents in situ reflectance FTIR spectra measured on MCMB electrode during the initial lithium intercalation process in P (VdF-HFP)-based gel electrolyte. Obvious changes are observed at potentials below 0.8 V. It was found that all the spectra recorded in the potential range of 0.8–0.02 V are similar with the same upward and downward peaks. Upward peaks at 1,818 and 1,281 cm^{-1} can be ascribed to $\tilde{\delta}_{c=0}$ and $\tilde{\delta}_{c-o-c}$, respectively, and those at 1,165 and 1,075 cm^{-1} both correspond to $\tilde{\delta}_{c-o}$ of EC [12, 20, 29], which indicates the decomposition of EC due to the polarization of the electrode. The downward peak at 1,680 cm^{-1} may correspond to $\tilde{\delta}_{c=0}$ of ROCO_2Li based on references [12, 20], which may suggest the formation of surface film. The other major downward peaks at 1,784, 1,726, 1,206, 1,094, and 849 cm^{-1} can be assigned to solvent subtraction (mostly EC) and the change by the solvation of lithium ion as reported in the reference [20]. Hence, Fig. 11 mainly indicates the depletion of EC during charging process. The strong absorption of solvent in the bulk phase may influence the interfacial information of surface film.

SEI formation on lithium electrode To avoid the contamination of impurities for lithium metal electrode in the cell-assembling process, lithium electrode was directly prepared by electrodeposition method within a sealed spectroelectrochemical cell with gel electrolyte. Metal lithium

Fig. 7 Selected Nyquist plots for MCMB electrode measured at different charge degree during the initial charge process in P (VdF-HFP)-based gel electrolyte

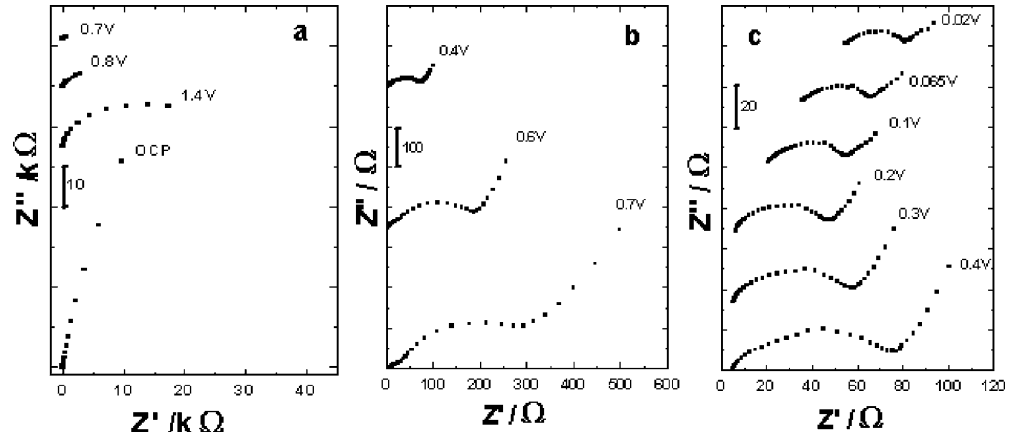
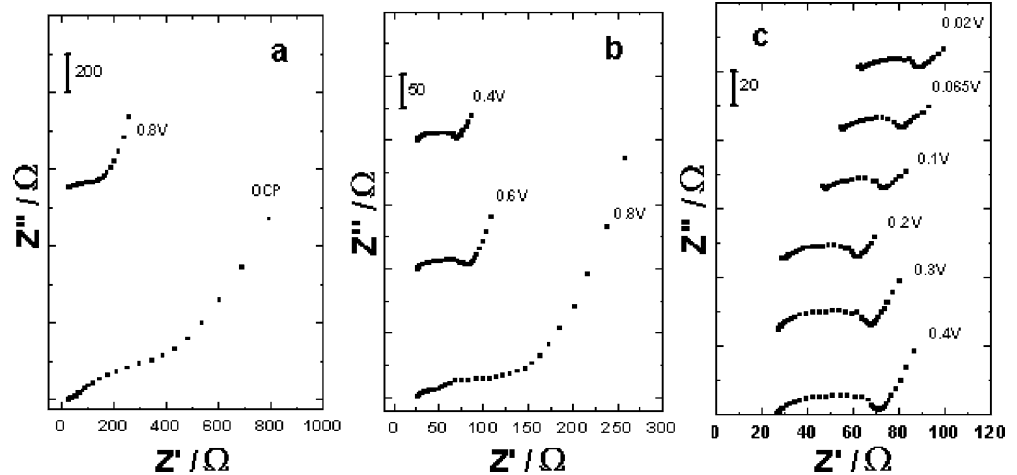


Fig. 8 Selected Nyquist plots for MCMB electrode measured at different charge degree during the fourth charge process in P (VdF-HFP)-based gel electrolyte



was electrochemically deposited on a copper substrate at -0.05 V for 5 min.

Curve a in Fig. 12 shows the selected in situ reflectance FTIR spectra recorded on the electrodeposited lithium electrode. Based on the spectra data of the reference [12], the bands at $1,522$, $1,428$, and 867 cm^{-1} can be attributed to Li_2CO_3 . Those bands at $1,705$, $1,567$, $1,488$, $1,315$, $1,189$, 905 , and 823 cm^{-1} can be assigned to ROCO_2Li and ROLi . The results of in situ FTIR spectra suggest that the surface film on lithium electrode formed in P (VdF-HFP)-based gel electrolyte mainly consists of ROCO_2Li , ROLi , and Li_2CO_3 .

For comparison, the in situ reflectance FTIR spectra at metal lithium foil electrode were detected as curve b in Fig. 12. It is interesting to note that the two spectra in Fig. 12 are very similar with almost the same upward and downward bands. As a result, it may be suggested that the electrodeposited metal lithium in the assembled spectroscopic-cell can be used as the investigative electrode instead of lithium foil electrode, which may be helpful to some experiments to avoid the reaction of lithium foil with some impurities during the cell assembling process.

Conclusions

Electrochemical techniques and in situ Raman and FTIR spectroscopic methods were used to investigate the interfacial reaction on MCMB electrode and lithium metal electrode in the prepared P (VdF-HFP)-based gel electrolyte. In situ Raman spectroscopy and charge-discharge

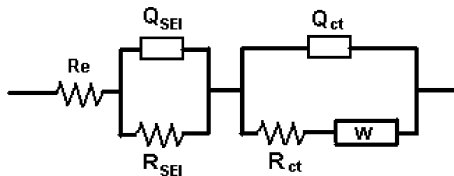


Fig. 9 Equivalent circuit chosen for analysis of impedance spectra for lithium intercalation into MCMB electrode in the prepared gel electrolyte. R and Q represent resistance and a CPE, respectively; W refers to Warburg resistance

profile prove that the structure changes of MCMB during lithium ions intercalation are through several stage transitions from dilute stage 1 to 4, 3, 2, and finally to 1. An initial irreversible capacity about 50 $\text{mA}\text{h}\text{g}^{-1}$ was observed in the initial charge-discharge cycle of MCMB

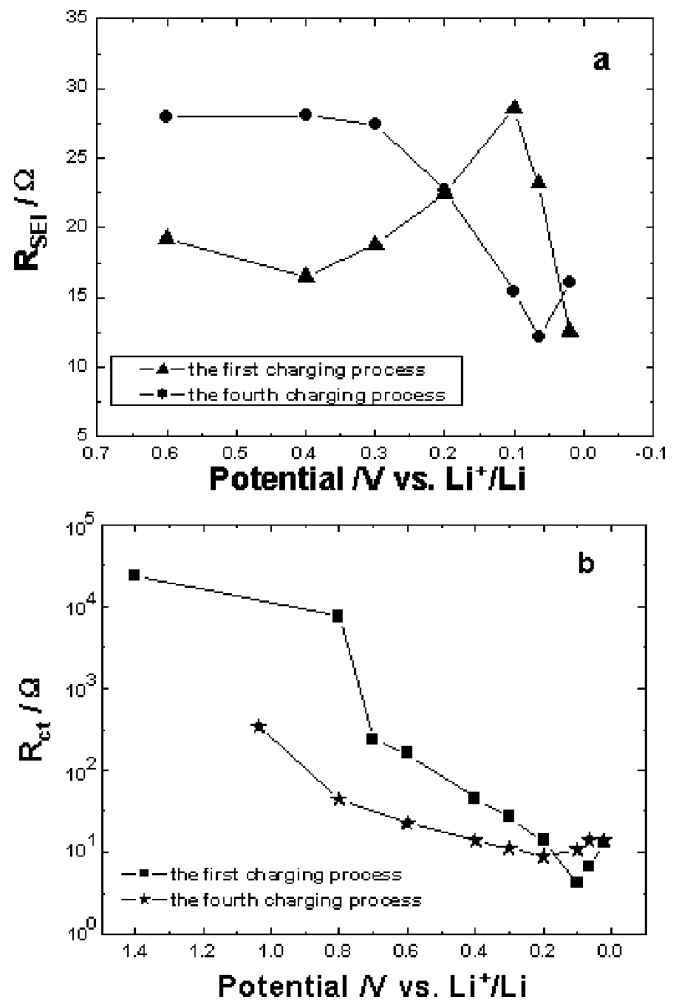


Fig. 10 Parameter values of R_{SEI} (a) and R_{ct} (b) obtaining from fitting the impedance spectra of MCMB electrode during the initial and fourth lithium intercalation, respectively

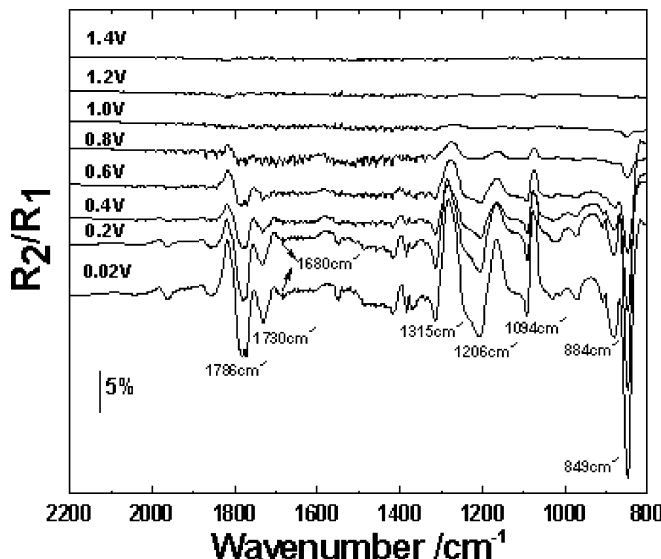


Fig. 11 In situ reflectance FTIR spectra of MCMB electrode during the initial lithium intercalation process in P (VdF-HFP)-based gel electrolyte

electrode. It can be ascribed to the consumption for the SEI formation on the MCMB surface, which was further confirmed by in situ FTIR spectroscopy and EIS measurements. In situ FTIR spectra for MCMB electrode during initial charging process mainly indicates the depletion of EC and may suggest the formation of ROCO_2Li . For metal lithium electrode, SEI film was composed by ROCO_2Li , ROLi and Li_2CO_3 , not electrodeposited or foil electrodes.

Acknowledgement The work was supported by National Nature Science Foundation of China.

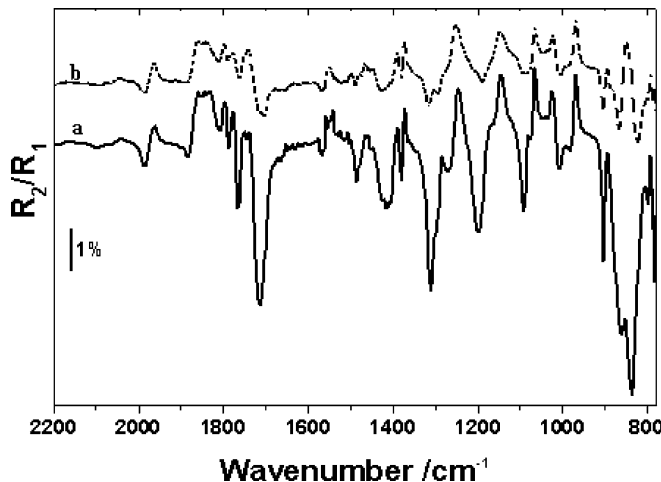


Fig. 12 The selected in situ reflectance FTIR spectra of electro-deposited Li electrode on Cu substrate (a) and Li metal electrode in P (VdF-HFP)-based gel electrolyte (b)

References

- Song JY, Wang YY, Wan CC (1999) *J Power Sources* 77:183
- Kono M, Nishiura M, Ishiko E, Sada T (2000) *Electrochim Acta* 45:1307
- Kim DW, Ko JM, Chun JH, Kim SH, Park JK (2001) *Electrochim Commun* 3:535
- Oh B, Amine K (2004) *Solid State Ionics* 175:785
- Yoshimoto N, Shirai T, Morita M (2005) *Electrochim Acta* 50:3866
- Lopes LVS, Machado GO, Pawlicka A, Donoso JP (2005) *Electrochim Acta* 50:3978
- Kumar GG, Sampath S (2005) *Solid State Ionics* 176:773
- Aurbach D, Zaban A (1994) *J Electrochem Soc* 141:1808
- Aurbach D, Zaban A, Chusid O, Weissman I (1994) *Electrochim Acta* 39:51
- Aurbach D, Zaban A, Gofer Y, Ein-Eli Y, Weissman I, Chusid O, Abramson O (1995) *J Power Sources* 54:76
- Aurbach D, Ein-Eli Y (1995) *J Electrochem Soc* 142:1746
- Aurbach D, Levi MD, Levi E, Schechter A (1997) *J Phys Chem B* 101:2195
- Ein-Eli Y, McDevitt SF (1997) *J Solid State Electrochem* 1:227
- Novák P, Joho F, Imhof R, Panitz JC, Haas O (1999) *J Power Sources* 81–82:212
- Bar-Tov D, Peled E, Burstein L (1999) *J Electrochem Soc* 146:824
- Inaba M, Kawatake Y, Funabiki A, Jeong SK, Abe T, Ogumi Z (1999) *Electrochim Acta* 45:99
- Novák P, Panitz JC, Joho F, Lanz M, Imhof R, Coluccia M (2000) *J Power Sources* 90:52
- Alliata D, Kötz R, Novák P, Siegenthaler H (2000) *Electrochim Commun* 2:436
- Novák P, Joho F, Lanz M, Rykart B, Panitz JC, Alliata D, Kötz R, Haas O (2001) *J Power Sources* 97–98:39
- Morigaki KI (2002) *J Power Sources* 103:253
- Lee S, Pyun SI (2003) *J Solid State Electrochem* 7:374
- Levi E, Lancry E, Gofer Y, Aurbach D (2006) *J Solid State Electrochem* 10:176
- Li X, Zhao Y, Cheng L, Yan M, Zheng X, Gao Z, Jiang Z (2005) *J Solid State Electrochem* 9:609
- Zhang S, Shi P (2004) *Electrochim Acta* 49:1475
- Levi MD, Aurbach D (1997) *J Phys Chem B* 101:4630
- Chang YC, Sohn HJ (2000) *J Electrochem Soc* 147:50
- Huang W, Frech R (1998) *J Electrochem Soc* 145:765
- Panitz JC, Joho F, Novák P (1999) *Appl Spectrosc* 53:1188
- Joho F, Novák P (2000) *Electrochim Acta* 45:3589
- Churikov AV, Gamayunova IM, Shirokov AV (2000) *J Solid State Electrochem* 4:216
- Umeda M, Dokko K, Fujita Y, Mohamedi M, Uchida I, Selman JR (2001) *Electrochim Acta* 47:885